International Journal of Thermal Sciences 160 (2021) 106673

Contents lists available at ScienceDirect

International Journal of Thermal Sciences

journal homepage: http://www.elsevier.com/locate/ijts

Temperature distribution in a multi-layer cylinder with circumferentially-varying convective heat transfer boundary conditions

Long Zhou [a,b], Mohammad Parhizi [b], Ankur Jain [b,*]

[a] School of Mechanical and Power Engineering, Henan Polytechnic University, Jiaozuo, Henan, China
[b] Mechanical and Aerospace Engineering Department University of Texas at Arlington, Arlington, TX, USA

ARTICLE INFO

Keywords:
Thermal conduction
Multilayer cylinder
Theoretical modeling
Convective heat transfer

ABSTRACT

Theoretical modeling of thermal conduction in a multilayer cylinder has been studied in multiple past papers due to its significance in engineering applications such as nuclear engineering, energy storage and sensing. Most past papers have assumed a constant convective heat transfer coefficient on the outer surface of the cylinder. However, a circumferentially varying heat transfer coefficient may be appropriate in several applications due to the distributed nature of fluid flow around the cylinder. This paper presents a theoretical model for steady-state thermal conduction in a multilayer cylinder with circumferentially-varying convective heat transfer coefficient on the cylinder surface. The theoretical model is presented for both solid and annular cylinders. A series solution is derived for the temperature distribution in each layer by using the convective boundary condition(s) to derive a set of linear algebraic equations for the coefficients of the inner-most layer. Results are shown to be in good agreement with numerical simulations and with closed-form solutions for special cases. The impact of various problem parameters, such as internal heat generation rate and thermal contact resistances on the temperature distribution is analyzed. It is expected that the results presented in this work will improve the theoretical understanding of multilayer heat transfer and be of practical use in multiple engineering applications.

1. Introduction

Heat transfer in a multilayer cylinder is a problem of significant engineering interest [1,2]. The use of a combination of materials with varying thermal/mechanical properties often helps provide desired performance characteristics for engineering structures and systems. For example, nuclear fuel rods in a nuclear reactor are often structured in the form of a multilayer cylinder, with the nuclear fuel packed in the annular region between two cylinders [3]. Other applications where thermal conduction in a multilayer cylinder is relevant include compressed hydrogen storage [4], superconducting cables [5], piezoelectric transducers [6] and civil engineering structures [7].

In each of these scenarios, heat generation in one or more concentric cylinders leads to temperature rise and stress development. Understanding the nature of thermal conduction in the multilayer cylinder is important for ensuring the performance, safety and reliability of such systems.

A significant body of literature already exists on the analysis of thermal conduction in multilayer cylinders. While numerical simulations offer the capability to rapidly compute the temperature distribution in a multilayer cylinder, analytical modeling is important for fully understanding the nature of thermal transport and for understanding the dependence of temperature field on various parameters of the problem. A number of theoretical methods have been presented for this purpose. The separation of variables (SOV) method has been used for modeling thermal conduction in cylindrical and spherical composite laminates [8,9]. Analytical solution for transient heat conduction in cylindrical multilayer composite laminates has been derived by combining the Laplace transformation method with the Thomas algorithm [10] and the separation of variable method [11]. The eigenfunction expansion method has been used to derive the general analytical solution for one-dimensional transient heat conduction in a three-layer cylinder [12]. A double-series solution for time-dependent asymmetric heat conduction in a multilayer annulus has been derived [13]. An analytical solution for transient heat conduction in hollow composite cylinders with an arbitrary number of layers and subject to general boundary conditions using the distributed transform function formulation has been derived [14]. The asymmetric thermal conduction problem in a multilayer annulus with time-dependent boundary conditions has been solved using the finite integral transform method [15]. Green's function method has been used to derive an analytical solution for

* Corresponding author. 500 W First St, Rm 211, Arlington, TX, 76019, USA .
E-mail address: jaina@uta.edu (A. Jain).

https://doi.org/10.1016/j.ijthermalsci.2020.106673
Received 3 June 2020; Received in revised form 18 September 2020; Accepted 6 October 2020
Available online 3 November 2020

Nomenclature

h_{in}	convective heat transfer coefficient at the inner surface (W/m^2K)
h_{out}	convective heat transfer coefficient at the outer surface (W/m^2K)
k	thermal conductivity (W/mK)
M	number of layers
N	number of eigenvalues
Q	internal heat generation rate (W/m^3)
R	thermal contact resistance (Km^2/W)
r	radial coordinate (m)
T	temperature rise (K)
θ	circumferential coordinate (rad)

thermal conduction in a two-layer hollow cylinder [16]. Fourier series expansion has also been used to obtain the temperature field for heat conduction in multilayer cylindrical composites [17,18]. In addition, enthalpy-based 3D hybrid finite element method has been used for solving anisotropic thermal conduction problems characterized by a set of tensors of thermal conductivity in different coordinate systems [19] and applied in a multi-layer material with multiple orientations of the thermal conductivity tensors [20]. In such problems, a linear coordinate transformation has been used to convert the anisotropic multi-layered heat conduction problem to the equivalent isotropic one, followed by Fourier transformation and series expansion technique to derive the closed-form solution [21].

Most of the literature relevant to thermal conduction in a multilayer cylinder applies a convective heat transfer boundary condition on the outer surface of the cylinder. This facilitates the modeling of, for example, heating or cooling due to the fluid flow external to the cylinder. However, in most papers, the convective heat transfer coefficient has been treated to be constant, whereas, there may be significant spatial variation in the convective heat transfer coefficient around the cylinder surface. For example, when considering cross-flow of a fluid past the cylinder, it is well-known [22,23] that the local Nusselt number *Nu* is a function of the circumferential location θ, in addition to being dependent on the Reynolds number, *Re*. The impact of the cross-flow is highest at the stagnation point $\theta = 0$ that directly faces the flow. As one traverses around the cylinder, boundary layer growth causes a reduction in *h*, followed by an increase due to onset of turbulence. Further changes occur in *h* with increasing θ due to separation and wake formation. The exact nature of the variation of *h* with θ, including the transition locations, depends on the value of *Re*, and has been widely studied [22,23]. It is important for accurate modeling of thermal conduction inside the multilayer cylinder to account for the variation of *h* with θ. Modeling a constant convective heat transfer coefficient around the cylinder is not accurate, and is likely to result in significant error in the predicted temperature distribution.

Unfortunately, treating the convective heat transfer coefficient to be a function of θ adds significant analytical complications. In the recent past, an analytical solution of thermal conduction with circumferentially varying convective heat transfer coefficient on the outer surfaces of a cylinder [24] and a sphere [25] has been presented. In this paper, the solution was written in the form of an infinite series – similar to the SOV approach for a constant *h* problem – and the coefficients for the series were shown to be governed by a set of coupled linear algebraic equations involving various integrals of *h(θ)*. The results presented in this paper were applicable only to a homogeneous cylinder. It is of both theoretical and practical interest to extend this method to a multi-layer cylinder. Such a result would be directly relevant for several engineering applications involving heat transfer in a multilayer cylinder, such as those summarized earlier in this section.

This paper presents an analytical solution for the two-dimensional temperature distribution in a multilayer cylinder subject to convective heat transfer coefficient on the outer surface that varies circumferentially around the cylinder. Results are derived for two specific cases – a solid, multilayer cylinder and an annular multilayer cylinder. In both cases, results are found to be in good agreement with numerical simulations and with standard solutions for simplified special cases. The impact of various problem parameters on the temperature distribution is analyzed using this model.

2. Analytical modeling

2.1. Solid cylinder

Consider thermal conduction in an *M*-layer, composite cylinder with circumferentially varying heat convective coefficient $h_{out}(\theta)$ on its outer surface, as shown in Fig. 1(a). The convective boundary condition could be a result of, for example, cross-flow of a fluid past the cylinder. Top-bottom symmetry in the imposed convective heat transfer coefficient, and therefore, in the resulting temperature distribution is assumed, as is expected to be the case for cross-flow of fluid past the cylinder. Therefore, only the top half of the cylinder ($0 \le \theta \le \pi$) is considered.

The radial size and thermal conductivity of each layer are (r_{i+1}-r_i) and k_i, respectively. Note that due to the solid nature of the cylinder, r_1=0. Uniform heat generation Q_i occurs in each layer. Further, an inter-layer thermal contact resistance R_i exists between the $(i\text{-}1)^{th}$ and i^{th} layers. In a cylindrical coordinate system, the governing steady state energy conservation equation for the i^{th} layer is expressed as:

$$\frac{k_i}{r}\frac{\partial}{\partial r}\left(r\frac{\partial T_i}{\partial r}\right)+\frac{k_i}{r^2}\frac{\partial^2 T_i}{\partial \theta^2}+Q_i=0\ (\mathrm{i}=1,2,\ldots,\mathrm{M}) \tag{1}$$

Boundary conditions for this problem are

$$\frac{\partial T_i}{\partial \theta}=0 \text{ at } \theta=0 \tag{2a}$$

$$\frac{\partial T_i}{\partial \theta}=0 \text{ at } \theta=\pi \tag{2b}$$

$$-k_M\frac{\partial T_M}{\partial r}=h_{out}(\theta)T_M \text{ at } r=r_{M+1} \tag{2c}$$

Interfacial boundary conditions accounting for temperature and heat flux continuity are

$$T_{i-1}(r,\theta)=T_i(r,\theta)-k_iR_i\frac{\partial T_i}{\partial r} \text{ at } r=r_i \tag{2d}$$

$$k_{i-1}\frac{\partial T_{i-1}}{\partial r}=k_i\frac{\partial T_i}{\partial r} \text{ at } r=r_i\ (i=2,3,\&,M) \tag{2e}$$

Equation (2d) represents temperature drop at the interface and is given by the product of the heat flux and thermal contact resistance. Equation (2e) represents conservation of heat flux at each interface. In addition to the boundary and interface conditions listed above, the temperature must also be finite at *r*=0.

The temperature field is first split into two parts as follows

$$T_i(r,\theta)=\varphi_i(r,\theta)-\frac{Q_ir^2}{4k_i} \tag{3}$$

By substituting Eq. (3) into Eqs. (1)-(2e), the following equations are derived for $\varphi_i(r,\theta)$:

$$\frac{1}{r}\frac{\partial}{\partial r}\left(r\frac{\partial \varphi_i}{\partial r}\right)+\frac{1}{r^2}\frac{\partial^2 \varphi_i}{\partial \theta^2}=0 \tag{4}$$

$$\frac{\partial \varphi_i}{\partial \theta}=0 \text{ at } \theta=0 \tag{5a}$$

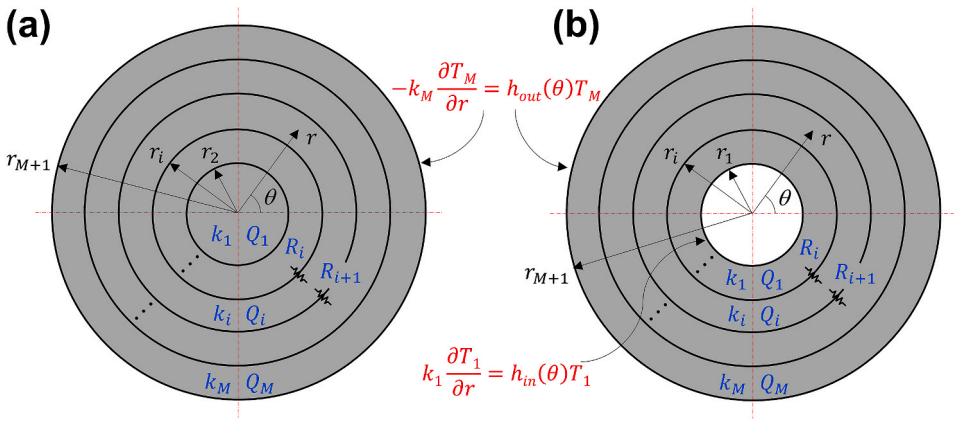

Fig. 1. Schematic of multilayer cylinder geometry: (a) Solid cylinder, (b) Annular cylinder.

$$\frac{\partial \varphi_i}{\partial \theta} = 0 \text{ at } \theta = \pi \tag{5b}$$

$$k_M \frac{\partial \varphi_M}{\partial r} + h_{out}(\theta)\varphi_M(r_{M+1},\theta) = F(\theta) \text{ at } r = r_{M+1} \tag{5c}$$

$$\varphi_{i-1}(r_i,\theta) = \varphi_i(r_i,\theta) + \frac{r_i^2}{4}\left(\frac{Q_{i-1}}{k_{i-1}} - \frac{Q_i}{k_i}\right) + \frac{r_i Q_i}{2} R_i - k_i R_i \frac{\partial \varphi_i}{\partial r} \text{ at } r = r_i \tag{5d}$$

$$k_{i-1}\frac{\partial \varphi_{i-1}}{\partial r} = k_i \frac{\partial \varphi_i}{\partial r} + \frac{r_i}{2}(Q_{i-1} - Q_i) \text{ at } r = r_i \tag{5e}$$

where

$$F(\theta) = \frac{Q_M r_{M+1}}{2}\left[1 + \frac{h_{out}(\theta) r_{M+1}}{2k_M}\right] \tag{6}$$

The solution for $\varphi_i(r,\theta)$ is derived next. Using Eqs. (4), (5a) and (5b), $\varphi_i(r,\theta)$ may be expressed as follows:

$$\varphi_1(r,\theta) = C_1 + \sum_{n=1}^{\infty} A_{1,n}\cos(n\theta)\left(\frac{r}{r_{M+1}}\right)^n \tag{7}$$

$$\varphi_i(r,\theta) = C_i + D_i \ln\left(\frac{r}{r_{M+1}}\right) + \sum_{n=1}^{\infty}\left[A_{i,n}\left(\frac{r}{r_{M+1}}\right)^n + B_{i,n}\left(\frac{r}{r_{M+1}}\right)^{-n}\right]\cos(n\theta) \text{ (i = 1, 2,…, M)} \tag{8}$$

Coefficients C_1, C_i, D_i, $A_{1,n}$, $A_{i,n}$ and $B_{i,n}$ must be determined in order to satisfy the outer boundary and interfacial conditions (5c), (5d) and (5e).

By substituting equations (7) and (8) into equations (5d) and (5e), one may obtain

$$C_i = C_1 + \frac{1}{4}\sum_{j=2}^{i} r_j^2\left(\frac{Q_j}{k_j} - \frac{Q_{j-1}}{k_{j-1}}\right) - \frac{1}{2}\sum_{j=2}^{i} r_j R_j Q_{j-1} - \frac{1}{2}\sum_{j=2}^{i}\frac{r_j^2}{k_j}(Q_j - Q_{j-1})\ln\left(\frac{r_j}{r_{M+1}}\right) - \frac{1}{2}\sum_{j=3}^{i}\left(\frac{1}{k_j} - \frac{1}{k_{j-1}}\right)\ln\left(\frac{r_j}{r_{M+1}}\right)\sum_{m=2}^{j-1} r_m^2(Q_m - Q_{m-1}) + \frac{1}{2}\sum_{j=3}^{i}\frac{R_j}{r_j}\sum_{m=2}^{j-1} r_m^2(Q_m - Q_{m-1}) \tag{9}$$

$$D_i = \frac{1}{2k_i}\sum_{j=2}^{i} r_j^2(Q_j - Q_{j-1}) \tag{10}$$

Further, $A_{i,n}$ and $B_{i,n}$ can be expressed using the following recursive relationship

$$A_{i,n} = \frac{1}{2}\left[1 + (1+\phi_{i,n})\frac{k_{i-1}}{k_i}\right]A_{i-1,n} + \frac{1}{2}\left[1 - (1+\phi_{i,n})\frac{k_{i-1}}{k_i}\right]B_{i-1,n}\left(\frac{r_i}{r_{M+1}}\right)^{-2n} \tag{11a}$$

$$B_{i,n} = \frac{1}{2}\left[1 - (1-\phi_{i,n})\frac{k_{i-1}}{k_i}\right]A_{i-1,n}\left(\frac{r_i}{r_{M+1}}\right)^{2n} + \frac{1}{2}\left[1 + (1-\phi_{i,n})\frac{k_{i-1}}{k_i}\right]B_{i-1,n} \tag{11b}$$

where $\phi_{i,n} = \frac{nk_i R_i}{r_i}$ and $B_{1,n} = 0$.

The two equations above can be further simplified to write $A_{i,n}$ and $B_{i,n}$ purely in terms of $A_{1,n}$ as follows

$$A_{i,n} = \eta_{i,A} A_{1,n} \tag{12a}$$

$$B_{i,n} = \eta_{i,B} A_{1,n} \tag{12b}$$

where the coefficients are given by the following coupled, recursive relationships:

$$\eta_{i,A} = \frac{1}{2}\left[1 + (1+\phi_{i,n})\frac{k_{i-1}}{k_i}\right]\eta_{i-1,A} + \frac{1}{2}\left[1 - (1+\phi_{i,n})\frac{k_{i-1}}{k_i}\right]\left(\frac{r_i}{r_{M+1}}\right)^{-2n}\eta_{i-1,B} \tag{13a}$$

$$\eta_{i,B}=\frac{1}{2}\left[1-\left(1-\phi_{i,n}\right)\frac{k_{i-1}}{k_i}\right]\left(\frac{r_i}{r_{M+1}}\right)^{2n}\eta_{i-1,A}+\frac{1}{2}\left[1+\left(1-\phi_{i,n}\right)\frac{k_{i-1}}{k_i}\right]\eta_{i-1,B} \tag{13b}$$

Note that $\eta_{1,A}=1$ and $\eta_{1,B}=0$

In the present case, while the summations in equation (18) involve, in principle, an infinite number of eigenvalues, the series are truncated at $n=N$ for computation. Integrating equation (18) from $\theta=0$ to $\theta=\pi$ and rearranging, one may obtain

$$C_1\int_0^{\pi}h_{out}(\theta)d\theta+\sum_{n=1}^{N}\left(\eta_{M,A}+\eta_{M,B}\right)\ A_{1,n}\int_0^{\pi}h_{out}(\theta)\cos(n\theta)d\theta=\int_0^{\pi}F(\theta)d\theta-\frac{\pi k_M D_M}{r_{M+1}}-g\int_0^{\pi}h_{out}(\theta)d\theta \tag{19}$$

Coefficients for the M^{th} layer are of particular interest. Setting $i=M$ in equations (9), (10), (12a) and (12b) yields

$$C_M=C_1+g \tag{14}$$

Also, multiplying both sides of equation (18) by $\cos(i\theta)$ for $i=1,2,\ldots,N$, and then integrating from $\theta=0$ to $\theta=\pi$ and rearranging results in

$$C_1\int_0^{\pi}h_{out}(\theta)\cos(i\theta)d\theta+\frac{i\pi k_M}{2r_{M+1}}\left(\eta_{M,A}-\eta_{M,B}\right)A_{1,i}\ +\sum_{n=1}^{N}\left(\eta_{M,A}+\eta_{M,B}\right)\ A_{1,n}\int_0^{\pi}h_{out}(\theta)\cos(n\theta)\cos(i\theta)d\theta=$$
$$\int_0^{\pi}F(\theta)\cos(i\theta)d\theta-g\int_0^{\pi}h_{out}(\theta)\cos(i\theta)d\theta \tag{20}$$

$$D_M=\frac{1}{2k_M}\sum_{j=2}^{M}r_j^2\left(Q_j-Q_{j-1}\right) \tag{15}$$

$$A_{M,n}=\eta_{M,A}A_{1,n} \tag{16a}$$

$$B_{M,n}=\eta_{M,B}A_{1,n} \tag{16b}$$

where

$$g=\frac{1}{4}\sum_{j=2}^{M}r_j^2\left(\frac{Q_j}{k_j}-\frac{Q_{j-1}}{k_{j-1}}\right)-\frac{1}{2}\sum_{j=2}^{M}r_jR_jQ_{j-1}-\frac{1}{2}\sum_{j=2}^{M}\frac{r_j^2}{k_j}\left(Q_j-Q_{j-1}\right)\ln\left(\frac{r_j}{r_{M+1}}\right)-$$
$$\frac{1}{2}\sum_{j=3}^{M}\left(\frac{1}{k_j}-\frac{1}{k_{j-1}}\right)\ln\left(\frac{r_j}{r_{M+1}}\right)\sum_{m=2}^{j-1}r_m^2\left(Q_m-Q_{m-1}\right)+\frac{1}{2}\sum_{j=3}^{M}\frac{R_j}{r_j}\sum_{m=2}^{j-1}r_m^2\left(Q_m-Q_{m-1}\right) \tag{17}$$

Equations (9)–(12b) express all the coefficients needed to define the temperature solution – C_i, D_i, $A_{i,n}$ and $B_{i,n}$ – in terms of C_1 and $A_{1,n}$ for each n.

In order to determine C_1 and $A_{1,n}$, and thus complete the solution, the temperature distribution in the outermost layer given by equation (8) is substituted into the boundary condition for the spatially varying heat transfer coefficient, equation (5c). Using expressions (14), (16a) and (16b), one can obtain

$$\frac{k_M D_M}{r_{M+1}}+\frac{k_M}{r_{M+1}}\sum_{n=1}^{\infty}n\left(\eta_{M,A}-\eta_{M,B}\right)\ A_{1,n}\cos(n\theta)+C_1h_{out}(\theta)+gh_{out}(\theta)+$$
$$\sum_{n=1}^{\infty}\left(\eta_{M,A}+\eta_{M,B}\right)\ A_{1,n}h_{out}(\theta)\cos(n\theta)=F(\theta) \tag{18}$$

The unknown coefficients C_1 and $A_{1,n}$ all appear in equation (18).

If the convective heat transfer coefficient was uniform, these coefficients can be easily determined using the principle of orthogonality.

Note that derivation of equation (20) used the orthogonality of the eigenfunctions

$$\sum_{n=1}^{\infty}\int_0^{\pi}\cos(n\theta)\cos(i\theta)d\theta=\begin{cases}0 & i\neq n\\ \pi/2 & i=n\end{cases} \tag{21}$$

Equations (19) and (20) represent $(N+1)$ linear algebraic equations involving $(N+1)$ unknowns, C_1 and $A_{1,i}$ $(i=1,2,\ldots,N)$. These equations can be easily solved using well-known methods such as matrix inversion based on LU factorization. Once these coefficients are determined, equation (3), along with equations (7), (8), (9), (10), (12a) and (12b) represents the final solution for temperature distribution in the composite body.

2.2. Annular cylinder

In this section, the thermal conduction problem is considered for a multilayer annular cylinder. Fig. 1(b) shows a schematic of the geometry for this problem. In this case, the convective heat transfer coefficients on the outer and inner surfaces – $h_{out}(\theta)$ and $h_{in}(\theta)$– are both spatially varying. The methodology for solving this problem is similar to the previous sub-section. The temperature distributions in each layer are written in series form. Using the interfacial conditions, coefficients for each layer are written in terms of the coefficients for the inner-most layer. Finally, the coefficients for the inner-most layer are determined through the use of the two spatially varying convective boundary conditions. This problem is still governed by equation (1) and boundary conditions (2a), (2b), (2c), (2d) and (2e). The convective boundary condition on the inner surface may be written as

$$k_1\frac{\partial T_1}{\partial r}=h_{in}(\theta)T_1 \text{ at } r=r_1 \tag{22a}$$

To start with, the non-homogeneity in the governing equation is removed using the same transformation used in the previous sub-section, resulting in Eqs. (3), (4) and (5a), (5b), (5d) and (5e).

Substituting Eq. (3) into Eqs. (22a) and (2b) results in

$$k_1\frac{\partial\varphi_1}{\partial r}-h_{in}(\theta)\varphi_1(r_1,\theta)=F_1(\theta)\text{ at }r=r_1 \tag{23a}$$

$$k_M\frac{\partial\varphi_M}{\partial r}+h_{out}(\theta)\varphi_M(r_{M+1},\theta)=F_M(\theta)\text{ at }r=r_{M+1} \tag{23b}$$

where

$$F_1(\theta)=\frac{Q_1 r_1}{2}\left[1-\frac{h_{in}(\theta)r_1}{2k_1}\right] \tag{24a}$$

$$F_M(\theta)=\frac{Q_M r_{M+1}}{2}\left[1+\frac{h_{out}(\theta)r_{M+1}}{2k_M}\right] \tag{24b}$$

The temperature distribution in each layer may be expressed as

$$\varphi_i(r,\theta)=C_i+D_i\ln\left(\frac{r}{r_{M+1}}\right)+\sum_{n=1}^{\infty}\left[A_{i,n}\left(\frac{r}{r_{M+1}}\right)^{n}+B_{i,n}\left(\frac{r}{r_{M+1}}\right)^{-n}\right]\cos(n\theta)\ (i=1,2,\ldots,M) \tag{25}$$

Note that since $r_1>0$, a separate equation for the temperature distribution in the inner-most layer – similar to the previous sub-section – is not needed here. The coefficients, C_iC_i, D_i, $A_{i,n}$ and $B_{i,n}$ must be determined in order to satisfy the boundary conditions (5d), (5e), (23a) and (23b).

By substituting equation (25) into equations (5d) and (5e), one may obtain

$$\begin{aligned}C_i=C_1+D_1k_1\sum_{j=2}^{i}\frac{R_j}{r_j}-D_1k_1\sum_{j=2}^{i}\left(\frac{1}{k_j}-\frac{1}{k_{j-1}}\right)\ln\left(\frac{r_j}{r_{M+1}}\right)-\frac{1}{2}\sum_{j=3}^{i}\left(\frac{1}{k_j}-\frac{1}{k_{j-1}}\right)\ln\left(\frac{r_j}{r_{M+1}}\right)\sum_{m=2}^{j-1}r_m^2(Q_m-Q_{m-1})+\\ \frac{1}{2}\sum_{j=3}^{i}\frac{R_j}{r_j}\sum_{m=2}^{j-1}r_m^2(Q_m-Q_{m-1})+\frac{1}{4}\sum_{j=2}^{i}r_j^2\left(\frac{Q_j}{k_j}-\frac{Q_{j-1}}{k_{j-1}}\right)-\frac{1}{2}\sum_{j=2}^{i}\frac{r_j^2}{k_j}(Q_j-Q_{j-1})\ln\left(\frac{r_j}{r_{M+1}}\right)-\frac{1}{2}\sum_{j=2}^{i}r_jR_jQ_{j-1}\end{aligned} \tag{26}$$

$$D_i=\frac{k_1}{k_i}D_1+\frac{1}{2k_i}\sum_{j=2}^{i}r_j^2(Q_j-Q_{j-1}) \tag{27}$$

Also, the coefficients $A_{i,n}$ and $B_{i,n}$ may be expressed in terms of $A_{1,n}$ and $B_{1,n}$ as follows

$$A_{i,n}=\eta_{i,A}A_{1,n}+\mu_{i,A}B_{1,n} \tag{28a}$$

$$B_{i,n}=\eta_{i,B}A_{1,n}+\mu_{i,B}B_{1,n} \tag{28b}$$

where the coefficients are given by Eqs. (13a) and (13b) as well as the following two expressions:

$$\mu_{i,A}=\frac{1}{2}\left[1+(1+\phi_{i,n})\frac{k_{i-1}}{k_i}\right]\mu_{i-1,A}+\frac{1}{2}\left[1-(1+\phi_{i,n})\frac{k_{i-1}}{k_i}\right]\left(\frac{r_i}{r_{M+1}}\right)^{-2n}\mu_{i-1,B} \tag{29a}$$

$$\mu_{i,B}=\frac{1}{2}\left[1-(1-\phi_{i,n})\frac{k_{i-1}}{k_i}\right]\left(\frac{r_i}{r_{M+1}}\right)^{2n}\mu_{i-1,A}+\frac{1}{2}\left[1+(1-\phi_{i,n})\frac{k_{i-1}}{k_i}\right]\mu_{i-1,B} \tag{29b}$$

Starting values for these recursive relationships are given by $\eta_{1,A}=1$ $\mu_{1,A}=0$, $\eta_{1,B}=0$ and $\mu_{1,B}=1$.

The coefficients for the M^{th} layer are of particular interest. Setting $i=M$ in equations (2), (26) and (27)8a) and (28b) yields

$$C_M=C_1+f_1D_1+f_2 \tag{30}$$

$$D_M=\frac{k_1}{k_M}D_1+g \tag{31}$$

$$A_{M,n}=\eta_{M,A}A_{1,n}+\mu_{M,A}B_{1,n} \tag{32a}$$

$$B_{M,n}=\eta_{M,B}A_{1,n}+\mu_{M,B}B_{1,n} \tag{32b}$$

where

$$f_1=k_1\sum_{j=2}^{M}\frac{R_j}{r_j}-k_1\sum_{j=2}^{M}\left(\frac{1}{k_j}-\frac{1}{k_{j-1}}\right)\ln\left(\frac{r_j}{r_{M+1}}\right) \tag{33a}$$

$$\begin{aligned}f_2=-\frac{1}{2}\sum_{j=3}^{M}\left(\frac{1}{k_j}-\frac{1}{k_{j-1}}\right)\ln\left(\frac{r_j}{r_{M+1}}\right)\sum_{m=2}^{j-1}r_m^2(Q_m-Q_{m-1})+\frac{1}{2}\sum_{j=3}^{M}\frac{R_j}{r_j}\sum_{m=2}^{j-1}r_m^2(Q_m-Q_{m-1})+\\ \frac{1}{4}\sum_{j=2}^{M}r_j^2\left(\frac{Q_j}{k_j}-\frac{Q_{j-1}}{k_{j-1}}\right)-\frac{1}{2}\sum_{j=2}^{M}\frac{r_j^2}{k_j}(Q_j-Q_{j-1})\ln\left(\frac{r_j}{r_{M+1}}\right)-\frac{1}{2}\sum_{j=2}^{M}r_jR_jQ_{j-1}\end{aligned} \tag{33b}$$

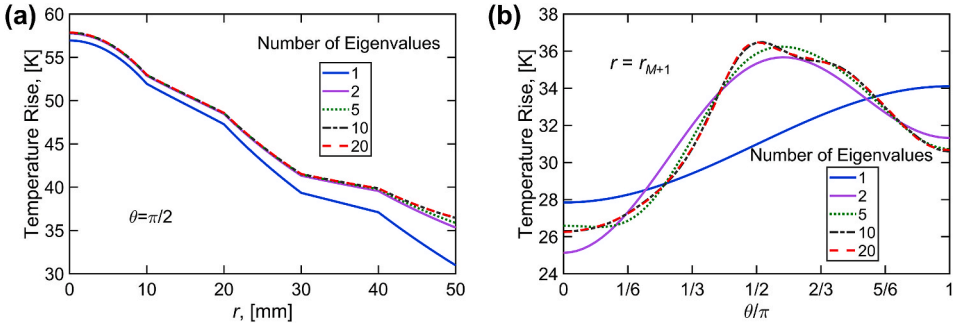

Fig. 2. Effect of number of eigenvalues: (a) Radial temperature distribution at $\theta = \pi/2$; (b) Circumferential temperature distribution on the outer surface for different number of eigenvalues for a five-layer problem. Problem parameters are shown in Table 1 . $h_{out}(\theta)$ is taken from *Nu* measurements around the cylinder for cross-flow of room temperature air at Re = 15,550 [23].

Table 1
List of problem parameters for the five-layer problem.

Layer #	Radial location (mm)	k (W/mK)	Q (W/m^3)	R (Km^2/W)
1	0–10	1	2×10^5	
2	10–20	2	6×10^4	2×10^{-4}
3	20–30	1	5×10^3	3×10^{-4}
4	30–40	3	2×10^4	10^{-4}
5	40–50	1	1×10^3	2×10^{-4}

$$g = \frac{1}{2k_M} \sum_{j=2}^{M} r_j^2 \left(Q_j - Q_{j-1}\right) \tag{33c}$$

Equations (13a), (13b), (26)-(29b) express all the coefficients needed to define the temperature solution – C_i, D_i, $A_{i,n}$ and $B_{i,n}$ – in terms of C_1, D_1, $A_{1,n}$ and $B_{1,n}$.

In order to determine C_1, D_1, $A_{1,n}$ and $B_{1,n}$, and thus complete the solution, equation (25) is separately substituted into the two boundary conditions involving spatially varying heat transfer coefficient, equations (23a) and (23b). Using expressions (30), (31), (32a) and (32b), one may obtain

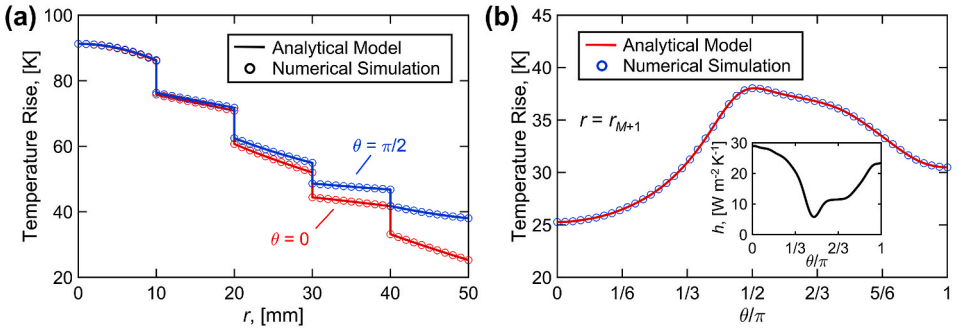

Fig. 3. Comparison of analytical model with numerical simulations for a five-layer solid cylinder: (a) Radial temperature distribution at $\theta = 0$ and $\theta = \pi/2$; (b) Circumferential temperature distribution on the outer surface. In both (a) and (b), results from analytical model (curves) and numerical simulation (symbols) are plotted. Problem parameters are the same as in Problem 2, with thermal contact resistance of $R = 0.01$ Km^2/W.

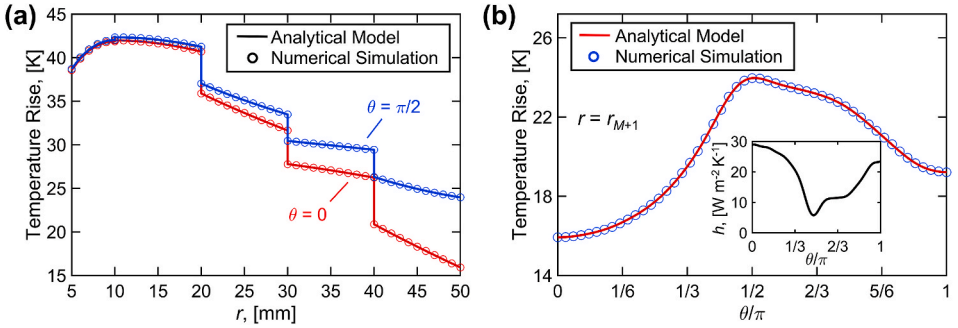

Fig. 4. Comparison of analytical model with numerical simulations for a five-layer annular cylinder: (a) Radial temperature distribution at $\theta = 0$ and $\theta = \pi/2$; (b) Circumferential temperature distribution on the outer surface. In both (a) and (b), results from analytical model (curves) and numerical simulation (symbols) are plotted. Problem parameters are the same as in Problem 2, with thermal contact resistance of $R = 0.01$ Km^2/W and $h_{in}(\theta) = 40$ W/m^{2}K.

$$\frac{k_1}{r_1}D_1+\frac{k_1}{r_1}\sum_{n=1}^{\infty}n\left[A_{1,n}\left(\frac{r_1}{r_{M+1}}\right)^n-B_{1,n}\left(\frac{r_1}{r_{M+1}}\right)^{-n}\right]\cos(n\theta)-C_1h_{in}(\theta)-D_1\ln\left(\frac{r_1}{r_{M+1}}\right)h_{in}(\theta)-$$
$$h_{in}(\theta)\sum_{n=1}^{\infty}\left[A_{1,n}\left(\frac{r_1}{r_{M+1}}\right)^n+B_{1,n}\left(\frac{r_1}{r_{M+1}}\right)^{-n}\right]\cos(n\theta)=F_1(\theta) \tag{34}$$

$$\frac{k_1}{r_{M+1}}D_1+\frac{k_M}{r_{M+1}}g+\frac{k_M}{r_{M+1}}\sum_{n=1}^{\infty}n(\eta_{M,A}-\eta_{M,B})\ A_{1,n}\cos(n\theta)+\frac{k_M}{r_{M+1}}\sum_{n=1}^{\infty}n(\mu_{M,A}-\mu_{M,B})\ B_{1,n}\cos(n\theta)+$$
$$C_1h_{out}(\theta)+f_1D_1h_{out}(\theta)+f_2h_{out}(\theta)+\sum_{n=1}^{\infty}(\eta_{M,A}+\eta_{M,B})\ A_{1,n}h_{out}(\theta)\cos(n\theta)+ \tag{35}$$
$$\sum_{n=1}^{\infty}(\mu_{M,A}+\mu_{M,B})\ B_{1,n}h_{out}(\theta)\cos(n\theta)=F_M(\theta)$$

Similar to the previous problem, the series sums in the equations above are truncated up to $n=N$ for the purpose of computation. Integrating equations (34) and (35) from $\theta=0$ to $\theta=\pi$ and rearranging, one may obtain

$$-C_1\int_0^{\pi}h_{in}(\theta)d\theta+\frac{\pi k_1}{r_1}D_1-D_1\ln\left(\frac{r_1}{r_{M+1}}\right)\int_0^{\pi}h_{in}(\theta)d\theta-\sum_{n=1}^{N}A_{1,n}\left(\frac{r_1}{r_{M+1}}\right)^n\int_0^{\pi}h_{in}(\theta)\cos(n\theta)d\theta-\sum_{n=1}^{N}B_{1,n}\left(\frac{r_1}{r_{M+1}}\right)^{-n}\int_0^{\pi}h_{in}(\theta)\cos(n\theta)d\theta=\int_0^{\pi}F_1(\theta)d\theta \tag{36}$$

$$C_1\int_0^{\pi}h_{out}(\theta)d\theta+\frac{\pi k_1}{r_{M+1}}D_1+f_1D_1\int_0^{\pi}h_{out}(\theta)d\theta+\sum_{n=1}^{N}(\eta_{M,A}+\eta_{M,B})\ A_{1,n}\int_0^{\pi}h_{out}(\theta)\cos(n\theta)d\theta+$$
$$\sum_{n=1}^{N}(\mu_{M,A}+\mu_{M,B})\ B_{1,n}\int_0^{\pi}h_{out}(\theta)\cos(n\theta)d\theta=\int_0^{\pi}F_M(\theta)d\theta-\frac{\pi k_M}{r_{M+1}}g-f_2\int_0^{\pi}h_{out}(\theta)d\theta \tag{37}$$

Also, multiplying both sides of equations (34) and (35) by $\cos(i\theta)$ for $i=1,2,\ldots,N$, and then integrating from $\theta=0$ to $\theta=\pi$ and rearranging results in

$$\begin{aligned}-C_1\int_0^{\pi}h_{in}(\theta)\cos(i\theta)d\theta-D_1\ln\left(\frac{r_1}{r_{M+1}}\right)\int_0^{\pi}h_{in}(\theta)\cos(i\theta)d\theta+\frac{i\pi k_1}{2r_1}A_{1,i}\left(\frac{r_1}{r_{M+1}}\right)^i\\-\frac{i\pi k_1}{2r_1}B_{1,i}\left(\frac{r_1}{r_{M+1}}\right)^{-i}-\sum_{n=1}^{N}A_{1,n}\left(\frac{r_1}{r_{M+1}}\right)^n\int_0^{\pi}h_{in}(\theta)\cos(n\theta)\cos(i\theta)d\theta\\-\sum_{n=1}^{N}B_{1,n}\left(\frac{r_1}{r_{M+1}}\right)^{-n}\int_0^{\pi}h_{in}(\theta)\cos(n\theta)\cos(i\theta)d\theta\\=\int_0^{\pi}F_1(\theta)\cos(i\theta)d\theta\end{aligned} \tag{38}$$

$$C_1\int_0^{\pi}h_{out}(\theta)\cos(i\theta)d\theta+f_1D_1\int_0^{\pi}h_{out}(\theta)\cos(i\theta)d\theta+\frac{i\pi k_M}{2r_{M+1}}(\eta_{M,A}-\eta_{M,B})A_{1,i}+$$
$$\frac{i\pi k_M}{2r_{M+1}}(\mu_{M,A}-\mu_{M,B})B_{1,i}+\sum_{n=1}^{N}(\eta_{M,A}+\eta_{M,B})\ A_{1,n}\int_0^{\pi}h_{out}(\theta)\cos(n\theta)\cos(i\theta)d\theta+ \tag{39}$$
$$\sum_{n=1}^{N}(\mu_{M,A}+\mu_{M,B})\ B_{1,n}\int_0^{\pi}h_{out}(\theta)\cos(n\theta)\cos(i\theta)d\theta=\int_0^{\pi}F_M(\theta)\cos(i\theta)d\theta-f_2\int_0^{\pi}h_{out}(\theta)\cos(i\theta)d\theta$$

Equations 36–39 represent $(2\ N+2)$ linear algebraic equations involving $(2\,N+2)$ unknowns, $C_1, D_1, A_{1,i}$ and $B_{1,i}$ $(i=1,2,\ldots,N)$. Similar to the previous problem, a solution of these coefficients through matrix inversion or a similar technique results in the final solution for temperature distribution in the multilayer annular cylinder, as given by equation (3), along with equations (25), (26), (27) (28a) and (28b).

3. Results and discussion

The effect of number of eigenvalues on the computed temperature distribution is examined first. This is important to do since the number of eigenvalues considered directly affects the computational time. On the other hand, the number of eigenvalues must be large enough to ensure accuracy. In general, the solution must converge as the number of eigenvalues increases. The threshold number of eigenvalues beyond which there is no significant change in the solution by considering further eigenvalues must be determined.

Fig. 2 plots the temperature distribution for a representative five-layer solid cylinder problem as a function of number of eigenvalues.

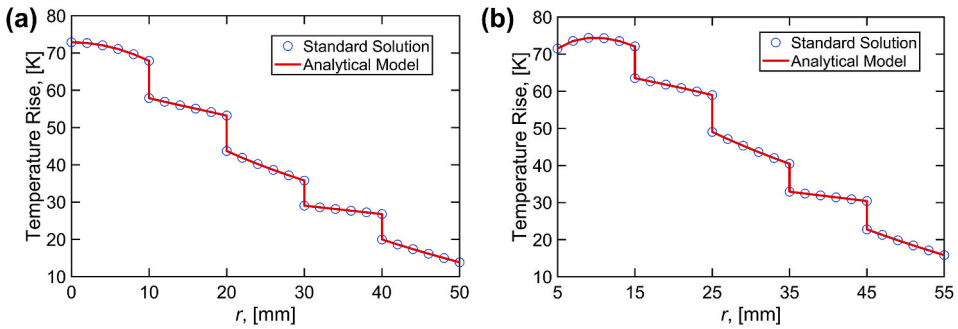

Fig. 5. Comparison of analytical model with standard solution for a special case with constant h, Q and R. Radial temperature distribution predicted by the analytical model and standard solution are plotted for (a) a solid cylinder and (b) an annular cylinder. For the annular cylinder, the inner-most radius is 5 mm and $h_{in} = 20$ W/m^{2}K.

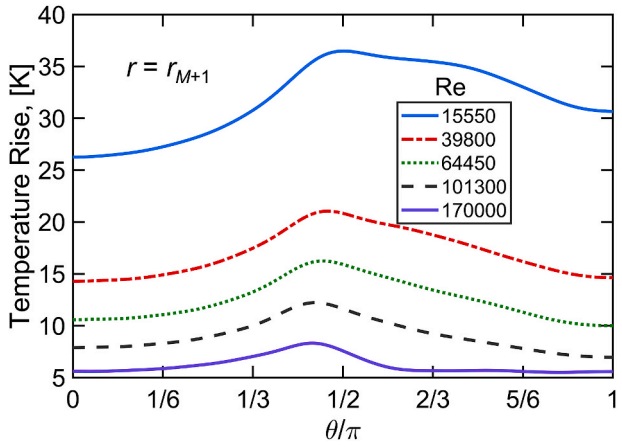

Fig. 6. Effect of Reynolds number on temperature distribution in a five-layer solid cylinder: Circumferential temperature distribution on the outer surface for five different values of *Re*. Other problem parameters are the same as Fig. 2.

The values of layer radii, thermal conductivities, heat generation rates and thermal contact resistances with neighboring layers are summarized in Table 1. The convective heat transfer coefficient on the outer surface is taken from past work by Schmidt & Wenner [23] that reported measurements of Nusselt number on the surface of a cylinder as a function of θ for a number of different values of Reynolds number. Re = 15,550 is assumed. Standard properties of air at room temperature are used to convert *Nu* into *h*. The outer diameter of the cylinder in the present work is the same as the one used in the past work. Note that while the Nusselt number measurements were presented by Schmidt & Wenner [23] as discrete data, a 17-term harmonic fit is used to represent h as a function of θ for different values of Re and evaluate the various integrals needed in the theoretical model. Equations for these harmonic fits are presented in Appendix A.

For these problem parameters, Fig. 2(a) and (b) plot the radial distribution of temperature rise at $\theta = \pi/2$ and the circumferential distribution on the outer surface, $r = r_{M+1}$, respectively. Results are plotted for 1, 2, 5, 10 and 20 eigenvalues. Both radial and circumferential plots show that while the results with only one eigenvalue are not accurate, there is rapid convergence thereafter. Even with two or five eigenvalues, the maximum error compared to the converged solution is less than 4.3% and 1.7%, respectively. Results with 10 and 20 eigenvalues nearly coincide with each other. This shows good convergence of the series solutions discussed in this work, and indicates that around ten eigenvalues provide sufficient accuracy and that use of additional eigenvalues is not necessary. All subsequent analysis in this work is carried out with ten eigenvalues.

In order to further validate the theoretical models developed in this work, results from the models are compared with finite-volume numerical simulations. The geometry of a five-layer body is created and meshed. A mesh with approximately 500000 elements is used for comparison with the theoretical model. The simulation uses 200 iterations and a residual target of 10^{-7}. Accuracy of the simulation is verified through mesh independence study. Further, it is verified that making the number of iterations or residual target more stringent does not affect the computed temperature distribution. All parameters in the simulation are the same as the theoretical model for Fig. 2, except the thermal contact resistance, for which, a value of 10^{-2} Km^2/W is considered at each interface. For this problem, Fig. 3(a) plots radial temperature distribution at $\theta = 0$ and $\theta = \pi/2$, while Fig. 3(b) plots the circumferential temperature distribution on the outer surface. In both Figures, results from the theoretical model in Section 2.1 are compared with numerical simulations. Fig. 3(a) and (b) show excellent agreement between the theoretical model and numerical simulations. The theoretical model is able to correctly capture the radial temperature distribution, including

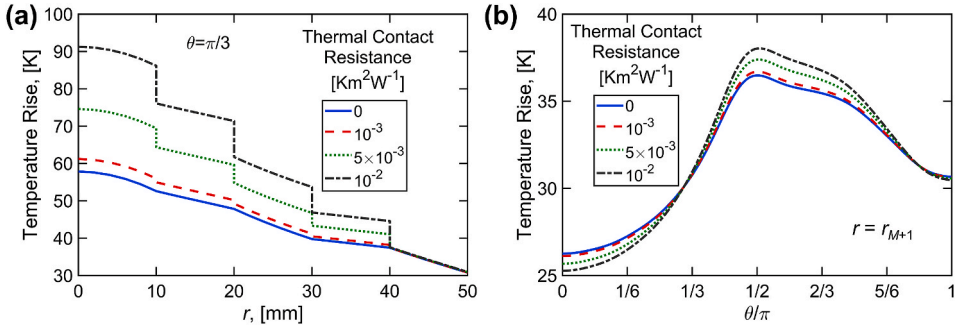

Fig. 7. Effect of thermal contact resistance on temperature distribution in a five-layer solid cylinder: (a) Radial temperature distribution at $\theta = \pi/3$, and (b) Circumferential temperature distribution on the outer surface for four different values of thermal contact resistance at each interface for the problem discussed in Fig. 2.

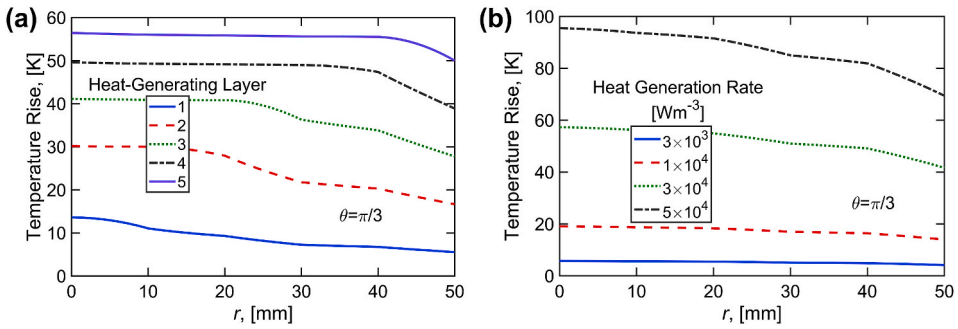

Fig. 8. Effect of heat generation rate: Radial temperature distribution for a five-layer solid cylinder at $\theta = \pi/3$ for two cases – (a) 10^5 W/m^3 in only one layer; (b) Heat generation of different magnitudes in all layers. Thermal contact resistance is neglected and all other parameters are the same as in Fig. 2.

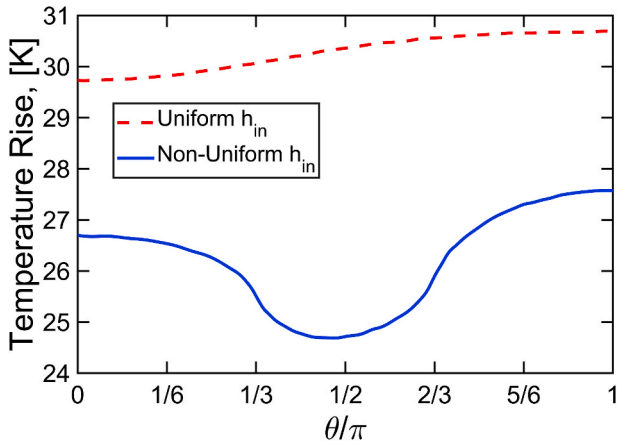

Fig. 9. Temperature distribution on the inner surface of a two-layer annular cylinder due to variable heat transfer coefficient applied on both inner and outer surfaces. For comparison, a baseline case is also plotted where the heat transfer coefficient on the inner surface is uniform.

discontinuities at interfaces for both $\theta = 0$ and $\theta = \pi/2$ directions. Similarly, the variation in the circumferential direction on the outer surface is correctly predicted by the theoretical model. As expected, Fig. 3(b) follows the expected trend in the temperature distribution based on the $h_{out}(\theta)$ function, which is shown in the inset. Temperature goes up when $h_{out}(\theta)$ goes down, and exhibits a maximum close to $\theta = \pi/2$, consistent with the minima in $h_{out}(\theta)$ at the same location.

A similar comparison between theoretical model and numerical simulation is carried out for the annular cylinder. In this case, the geometry and other problem parameters are identical to those considered in Fig. 3, except that the inner-most cylinder lies between $r = 5$ mm and $r = 10$ mm. A constant heat transfer coefficient $h_{in} = 40$ W/m^{2}K is modeled on the inner surface at $r = 5$ mm. The resulting radial and circumferential temperature distributions based on the theoretical model are shown in Fig. 4(a) and (b), respectively, and compared with numerical simulations. These Figures show excellent agreement between the two. Similar to Fig. 3(b), the circumferential temperature distribution in Fig. 4(b) also shows the expected trends based on the $h_{out}(\theta)$ distribution. A key difference between the solid cylinder and annular cylinder results shown in Figs. 3 and 4, respectively, is in the slope of the radial temperature distribution at $r = 0$. While this slope is zero for the solid cylinder, the slope on the inner surface, $r = 5$ mm for the annular case is clearly non-zero, which is due to the presence of the convective boundary condition on the inner surface of the multilayer cylinder.

For further validation of the theoretical model, results are compared with an analytical solution for a simplified case. For constant convective heat transfer coefficients, both the problems considered here become one-dimensional. The temperature rise as a function of r can be written for the solid cylinder as

$$\begin{cases} T_1(r) = -\dfrac{Q_1}{4k_1}r^2 + d_1 \\ T_i(r) = -\dfrac{Q_i}{4k_i}r^2 + c_i \ln(r) + d_i \quad (i = 2,3,4,5) \end{cases} \tag{40}$$

where

$$c_i = \frac{1}{2k_i}\sum_{j=2}^{i} r_j^2\left(Q_j - Q_{j-1}\right) \quad (i = 2,3,4,5) \tag{41a}$$

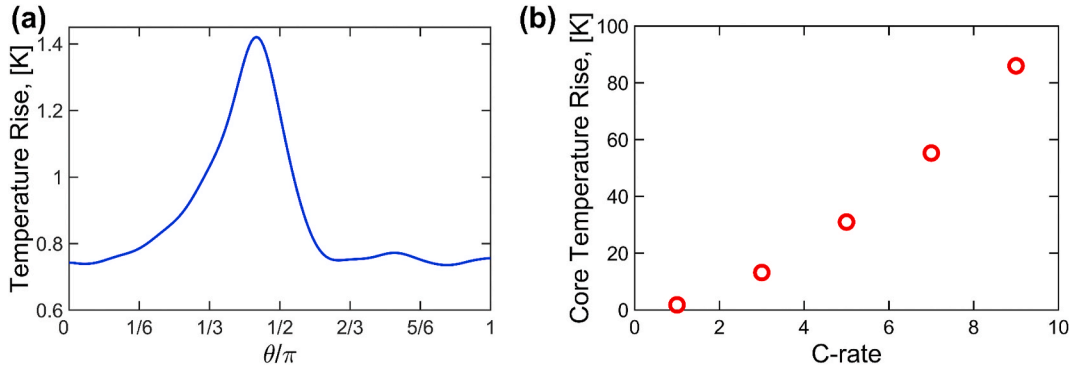

Fig. 10. Temperature field in a cylindrical Li-ion cell surrounded by insulation material: (a) Circumferential temperature distribution on the outer surface at a discharge rate of 3; (b) Core temperature rise in the Li-ion cell as a function of discharge rate.

$$d_1 = \frac{1}{4}\sum_{j=2}^{5} r_j^2\left(\frac{Q_{j-1}}{k_{j-1}} - \frac{Q_j}{k_j}\right) + \frac{1}{2}\sum_{j=2}^{5} R_j Q_j r_j - \sum_{j=2}^{4} c_j \ln(r_{j+1}) + \sum_{j=2}^{5} c_j\left[\ln(r_j) - \frac{k_j R_j}{r_j}\right] + d_5 \tag{41b}$$

$$d_i = \frac{1}{4}\sum_{j=i+1}^{5} r_j^2\left(\frac{Q_{j-1}}{k_{j-1}} - \frac{Q_j}{k_j}\right) + \frac{1}{2}\sum_{j=i+1}^{5} R_j Q_j r_j - \sum_{j=i}^{4} c_j \ln(r_{j+1}) + \sum_{j=i+1}^{5} c_j\left[\ln(r_j) - \frac{k_j R_j}{r_j}\right] + d_5 \quad (i = 2,3,4) \tag{41c}$$

$$d_5 = \frac{Q_5 r_6^2}{4k_5} + \frac{Q_5 r_6}{2h_{out}} - c_5\left[\ln(r_6) + \frac{k_5}{r_6 h_{out}}\right] \tag{41d}$$

and for the annular cylinder as

$$T_i(r) = -\frac{Q_i}{4k_i}r^2 + c_i \ln(r) + d_i \quad (i = 1,2,3,4,5) \tag{42}$$

where

$$c_1 = \frac{\beta_2}{\alpha_2} - \frac{h_{out}(\alpha_2\beta_1 - \alpha_1\beta_2)}{\alpha_2(h_{in}\alpha_2 - h_{out}\alpha_1)} \tag{43a}$$

$$d_1 = \frac{\alpha_2\beta_1 - \alpha_1\beta_2}{h_{in}\alpha_2 - h_{out}\alpha_1} \tag{43b}$$

$$c_i = f_i c_1 + g_i \quad (i = 2,3,4,5) \tag{43c}$$

$$d_i = u_i c_1 + d_1 + w_i \quad (i = 2,3,4,5) \tag{43d}$$

here

$$\alpha_1 = h_{in}\ln(r_1) - \frac{k_1}{r_1} \tag{44a}$$

$$\beta_1 = -\frac{Q_1 r_1}{2} + \frac{h_{in} Q_1 r_1^2}{4k_1} \tag{44b}$$

$$\alpha_2 = h_{out} f_5 \ln(r_6) + h_{out} u_5 + \frac{k_5 f_5}{r_6} \tag{44c}$$

$$\beta_2 = \frac{Q_5 r_6}{2} + \frac{h_{out} Q_5 r_6^2}{4k_5} - \frac{k_5 g_5}{r_6} - h_{out} g_5 \ln(r_6) - h_{out} w_5 \tag{44d}$$

$$f_i = \frac{k_1}{k_i} \tag{44e}$$

$$g_i = \frac{1}{2k_i}\sum_{j=2}^{i} r_j^2 (Q_j - Q_{j-1}) \tag{44f}$$

$$u_i = k_1 \sum_{j=2}^{i} \frac{R_j}{r_j} - k_1 \sum_{j=2}^{i}\left(\frac{1}{k_j} - \frac{1}{k_{j-1}}\right)\ln(r_j) \tag{44g}$$

$$w_i = \tfrac{1}{4}\sum_{j=2}^{i} r_j^2\left(\tfrac{Q_j}{k_j} - \tfrac{Q_{j-1}}{k_{j-1}}\right) + \tfrac{1}{2}\sum_{j=2}^{i}\tfrac{R_j}{r_j}\sum_{m=2}^{j} r_m^2(Q_m - Q_{m-1}) - \tfrac{1}{2}\sum_{j=2}^{i} R_j Q_j r_j$$
$$-\frac{1}{2}\sum_{j=2}^{i}\frac{\ln(r_j)}{k_j}\sum_{m=2}^{j} r_m^2(Q_m - Q_{m-1}) + \frac{1}{2}\sum_{j=2}^{i-1}\frac{\ln(r_{j+1})}{k_j}\sum_{m=2}^{j} r_m^2(Q_m - Q_{m-1}) \tag{44h}$$

Fig. 5 compares the radial temperature distribution determined from the theoretical models in Sections 2.1 and 2.2 with closed-form solutions given by equations (40) and (42) for this special case with $h_{out} = 40$ W/m^{2}K for both solid and annular cylinder, and, in addition, $h_{in} = 20$ W/m^{2}K for the annular cylinder. There is excellent agreement between the two for both cases.

The theoretical model is then used for investigating the effect of various problem parameters on the predicted temperature distribution. Fig. 6 plots the circumferential temperature distribution on the outer surface of the multilayer cylinder for five different values of *Re*. In each case, the $h_{out}(\theta)$ function is obtained from previously reported Nusselt number measurements around a cylinder of the same outer radius [23]. Standard properties of air at room temperature are used for obtaining $h_{out}(\theta)$ from *Nu*. Fig. 6 shows, as expected, that for each *Re*, the temperature distribution follows the expected trends in keeping with the distribution of the convective heat transfer coefficient around the cylinder. The temperature distribution is highest for the smallest value of *Re*, for which *Nu* and $h_{out}(\theta)$ are the lowest. A maxima is observed in each case, just prior to $\theta = \pi/2$, which is consistent with a minima in $h_{out}(\theta)$ at the same location.

The effect of thermal contact resistance between the layers is investigated using the theoretical model. Results are shown in Fig. 7 for four different cases. In each case, a constant thermal contact resistance is assumed at each interface, including the baseline case with no thermal contact resistance. Other problem parameters are the same as for Fig. 2. The radial and circumferential distributions of temperature rise for these cases are shown in Fig. 7. As expected, the case with zero thermal contact resistance shows continuous temperature distributions in the five regions. As shown in Fig. 7(a), the greater the thermal contact resistance, the larger is the temperature discontinuity. Fig. 7(a) also shows that for any given case, the temperature discontinuity is the largest on the innermost interface and smallest on the outermost interface. This is because even though the heat passing through the outermost interface is the largest, the heat flux is lower due to the much larger surface area. In contrast, heat flux across the innermost interface is the largest due to the lowest surface area, and therefore, the temperature discontinuity due to thermal contact resistance is the largest. In contrast to the strong dependence of radial temperature distribution on the thermal contact resistance, there is relatively weaker impact of the thermal contact resistance on temperature distribution on the outer surface of the cylinder. Fig. 7(b) shows around 4.3% change in the peak temperature rise for the highest thermal contact resistance considered here compared to the baseline case. This is likely because temperature on the outer surface is influenced more by the local convective heat transfer coefficient than the thermal contact resistances inside the cylinder. Moreover, despite the different thermal contact resistances, the net outward heat flux in steady state is the same for the four cases.

Finally, the effect of internal heat generation is investigated. Two specific problems of interest are solved for the five-layer geometry using the theoretical model. In the first problem, five different cases are compared in which only one specific layer generates heat at a constant rate of 10^5 W/m^3. In the second case, four different cases are considered, in which, all five layers generate varying amounts of heat. The temperature distributions for these cases are shown in Fig. 8(a) and (b), respectively, which plot the radial temperature distribution at $\theta = \pi/3$. In the first case, the temperature distribution is the largest when heat generation is in the outermost layer. Even though the outermost layer is closest to the cooling surface and the heat generation rate is the same for all five cases considered, this is attributable to the largest volume of the outer-most layer. As shown in Fig. 8(b), when all layers generate heat, the temperature rise goes up with increasing magnitude of the heat

generation rate. Note that Fig. 8(a) and (b) do not show temperature discontinuity between layers, which is because thermal contact resistance is not considered in these problems.

Fig. 9 plots temperature distribution on the inner surface of a two-layer annular cylinder where variable heat transfer coefficient is applied on both boundaries. In this case, the heat transfer coefficient applied on the outer surface corresponds to the Nusselt number for Re = 15,550 given in Appendix A, whereas the heat transfer coefficient applied on the inner surface is a top hat function, with a value of 80 W/m^{2}K between $\theta = \pi/3$ and $\theta = 2\pi/3$, and 40 W/m^{2}K elsewhere. The inner cylinder extends from $r = 5$ mm to $r = 10$ mm, and the outer cylinder from $r = 10$ mm to $r = 20$ mm. Thermal conductivities are taken to be 1 and 2 W/mK, respectively. Heat generation rates are 2×10^5 and 6×10^4 W/m^3, respectively. Thermal contact resistance of 0.01 Km^2/W is assumed. For comparison, temperature distribution is also plotted for a case with the same outer surface heat transfer coefficient and a constant 40 W/m^{2}K inner heat transfer coefficient (baseline case). As shown in Fig. 9, there is reduced temperature between $\theta = \pi/3$ and $\theta = 2\pi/3$ compared to the baseline case due to the greater local heat transfer coefficient. Interestingly, temperature in other regions is also lower than the baseline case. Note that there is circumferential variation in temperature even for the baseline case where the inner heat transfer coefficient is constant, because the outer heat transfer coefficient still has θ-dependence.

Finally, the application of the theoretical model for solving a practical thermal management problem is discussed. Specifically, temperature distribution in a cylindrical Li-ion cell of 18 mm diameter surrounded by a 3 mm thick insulation layer is computed. The cell is assumed to generate heat at a rate determined by its discharge rate [26]. Thermal properties of the cell are taken from past work [27] and standard properties of polypropylene are used for the insulation layer. The two-layer cylinder is assumed to be cooled by cross-flow of air at Re = 170,000. The circumferential variation in h is obtained from Appendix A. Fig. 10(a) plots the circumferential temperature distribution at the cell-insulation interface for a discharge rate (C-rate) of 3. Further, Fig. 10(b) plots peak temperature rise in the cell as a function of the discharge rate. As expected, temperature goes up as the discharge rate increases due to the quadratic dependence of heat generation rate on discharge rate [26]. Further, the circumferential variation in the temperature distribution is clearly seen in Fig. 10(a) due to the variation in the local convective heat transfer coefficient around the cylinder. A minima in h around $\theta = 80^\circ$ is seen to result in a corresponding peak in temperature at the same location. These Figures demonstrate the capability of the theoretical model presented here to analyze thermal conduction in practical engineering problems involving multilayer cylinders.

4. Conclusions

The analytical model presented in this paper addresses the important problem of circumferentially-varying convective heat transfer on the surface of a multi-layer cylinder. The solution is derived in a form of an infinite series for each layer. Relationships between coefficients of various layers are derived, and the coefficients for the inner-most layer are shown to be governed by a set of algebraic equations. The resulting temperature distribution is shown to be in agreement with numerical simulations. The present model is used for parametric study of thermal conduction in multilayer cylinders of practical relevance. This work improves upon past theoretical models in which the heat transfer coefficient is treated to be uniform, whereas in realistic conditions, there may be significant spatial variation. In addition, the solution methodology makes it possible to account for internal heat generation and thermal contact resistance between layers. These models improve our understanding of thermal conduction in multilayer cylindrical geometry. In addition, the solid and annular cylinder models presented in this work may help understand and improve the thermal performance of a variety of engineering systems.

CRediT authorship contribution statement

Long Zhou: Methodology, Formal analysis, Investigation, Data curation, Visualization, Writing - original draft, Writing - review & editing. **Mohammad Parhizi:** Formal analysis, Data curation, Visualization, Writing - original draft, Writing - review & editing. **Ankur Jain:** Conceptualization, Methodology, Supervision, Project administration, Visualization, Writing - original draft, Writing - review & editing.

Declaration of competing interest

The authors declare that they have no known competing financial interests or personal relationships that could have appeared to influence the work reported in this paper.

Acknowledgments

This material is based upon work supported by CAREER Award No. CBET-1554183 from the National Science Foundation. This research was supported by the Key Project of Science of the Education Bureau of Henan Province (19B460005), Special Project of Basic Scientific Research Operating Expenses of Henan Polytechnic University (NSFRF180427), and China Scholarship Council.

Appendix A. Curve fits for *Nu(θ)* for various values of *Re*

Discrete measurement data for Nu around the cylinder reported by Schmidt & Wenner [23] for various values of Re are curve-fit with a 17-term harmonic equation. The resulting equations and parameter values are given below:

$$Nu(\theta) = (a_0 + a_1\cdot\cos(\theta\cdot\omega) + b_1\cdot\sin(\theta\cdot\omega) + a_e\cdot\cos(2\cdot\theta\cdot\omega) + b_2\cdot\sin(2\cdot\theta\cdot\omega) + a_3\cdot\cos(3\cdot\theta\cdot\omega) + b_3\cdot\sin(3\cdot\theta\cdot\omega) + a_4\cdot\cos(4\cdot\theta\cdot\omega) + b_4\cdot\sin(4\cdot\theta\cdot\omega) + a_5\cdot\cos(5\cdot\theta\cdot\omega) + b_5\cdot\sin(5\cdot\theta\cdot\omega) + a_6\cdot\cos(6\cdot\theta\cdot\omega) + b_6\cdot\sin(6\cdot\theta\cdot\omega) + a_7\cdot\cos(7\cdot\theta\cdot\omega) + b_7\cdot\sin(7\cdot\theta\cdot\omega) + a_8\cdot\cos(8\cdot\theta\cdot\omega) + b_8\cdot\sin(8\cdot\theta\cdot\omega)) \quad \text{(A1)}$$

Where.

(a) Re = 15,550

$a_0 = 78.89$; $e = 40.47$; $b_1 = 10.68$; $a_2 = -3.924$; $b_2 = 5.205$; $a_3 = -0.07861$; $e = -5.816$; $a_4 = 2.779$; $b_4 = 5.291$; $a_5 = -0.8624$; $b_5 = -1.182$; $a_6 = 2.533$; $b_6 = 0.1599$; $a_7 = -0.1826$; $b_7 = -0.1108$; $a_8 = 0.663$; $b_8 = -0.9456$; $\omega = 0.03151$;

(a) Re = 39,800

$a_0 = 142.7$; $a_1 = 64.03$; $b_1 = 7.351$; $a_2 = -9.513$; $b_2 = 3.944$; $a_3 = 3.17$; $b_3 = -10.9$; $a_4 = -0.5481$; $b_4 = 4.798$; $a_5 = -2.037$; $b_5 = -4.906$; $a_6 = 1.165$; $b_6 = 1.916$; $a_7 = -1.989$; $b_7 = -1.437$; $a_8 = 1.406$; $b_8 = 0.1572$; $\omega = 0.03387$;

(c) Re = 64,450

$a_0 = 199.7$; $a_1 = 84.7$; $b_1 = -18.89$; $a_2 = -14.66$; $b_2 = 5.808$; $a_3 = -5.415$; $b_3 = -18.61$; $a_4 = 0.1731$; $b_4 = 5.86$; $a_5 = -5.586$; $b_5 = -1.469$; $a_6 = 2.664$; $b_6 = -1.669$; $a_7 = -2.843$; $b_7 = 1.000$; $a_8 = -0.3577$; $b_8 = -2.404$; $\omega = 0.03219$;

(d) Re = 101,300

$a_0 = 276.4$; $a_1 = 94.87$; $b_1 = -50.58$; $a_2 = -16.56$; $b_2 = 12.45$; $a_3 = -11.2$; $b_3 = -24.89$; $a_4 = 2.457$; $b_4 = 4.946$; $a_5 = -9.306$; $b_5 = -0.6281$; $a_6 = 1.242$; $b_6 = -4.341$; $a_7 = -2.698$; $b_7 = 3.37$; $a_8 = -2.892$; $b_8 = -2.799$; $\omega = 0.0316$;

(e) Re = 170,000

$a_0 = 372.4$; $a_1 = 94.49$; $b_1 = -9.922$; $a_2 = -54.39$; $b_2 = 1.607$; $a_3 = 24.47$; $b_3 = 21.48$; $a_4 = -3.755$; $b_4 = -10.97$; $a_5 = 1.185$; $b_5 = 6.927$; $a_6 = 0.4804$; $b_6 = -0.9187$; $a_7 = 2.368$; $b_7 = 1.704$; $a_8 = -2.087$; $b_8 = -2.066$; $\omega = 0.04103$; Note that θ is in degrees.

References

[1] D.W. Hahn, M.N. Özişik, Heat Conduction, 3rd. Ed., John Wiley & Sons, 2012.
[2] S. Kakaç, Y. Yener, Heat Conduction, 2nd. Ed., Hemisphere Press, 1985.
[3] H. French, Heat Transfer and Fluid Flow in Nuclear Systems, ' first ed., Pergamon Press, 1981.
[4] S. Manahan, Environmental Chemistry, ' ninth ed., CRC Press, 2010.
[5] S. Olsen, C. Traeholt, A. Kuhle, O. Tonnesen, M. Daumling, J. Oestergaard, Loss and inductance investigations in a 4-layer superconducting prototype cable conductor, IEEE Trans. Appl. Supercond. 9 (1999) 833–836.
[6] J. Wang, L. Qin, W. Li, W. Song, Parametric analysis and optimization of radially layered cylindrical piezoceramic/epoxy composite transducers, Micromachines 9 (2018), 585:1-16.
[7] M. Cavalcante, S. Marques, M.-J. Pindera, Transient thermomechanical analysis of a layered cylinder by the parametric finite-volume theory, J. Therm. Stresses 32 (2008) 112–134.
[8] M.H. Kayhani, M. Shariati, M. Norouzi, M. Karimi Demneh, Exact solution of conductive heat transfer in cylindrical composite laminate, Heat Mass Tran. 46 (2009) 83–94.
[9] M. Norouzi, A. Amiri Delouei, M. Seilsepour, A general exact solution for heat conduction in multilayer spherical composite laminates, Compos. Struct. 106 (2013) 288–295.
[10] A. Amiri Delouei, M.H. Kayhani, M. Norouzi, Exact analytical solution of unsteady axi-symmetric conductive heat transfer in cylindrical orthotropic composite laminates, Int. J. Heat Mass Tran. 55 (2012) 4427–4436.
[11] M. Norouzi, S.M. Rezaei Niya, M.H. Kayhani, M. Shariati, M. Karimi Demneh, M. S. Naghavi, Exact solution of unsteady conductive heat transfer in cylindrical composite laminates, J. Heat Tran. 134 (2012), 101301:1-10.
[12] F. de Monte, An analytic approach to the unsteady heat conduction processes in one-dimensional composite media, Int. J. Heat Mass Tran. 45 (2002) 1333–1343.
[13] P.K. Jain, S. Singh, Rizwan-uddin, 'Analytical solution to transient asymmetric heat conduction in a multilayer annulus', J. Heat Tran. 131 (2009), 011304-1-011304-7.
[14] B. Yang, S. Liu, Closed-form analytical solutions of transient heat conduction in hollow composite cylinders with any number of layers, Int. J. Heat Mass Tran. 108 (2017) 907–917.
[15] S. Singh, P.K. Jain, Rizwan-uddin, Finite integral transform method to solve asymmetric heat conduction in a multilayer annulus with time-dependent boundary conditions, Nucl. Eng. Des. 241 (2011) 144–154.
[16] S. Kukla, U. Siedlecka, 'Heat conduction problem in a two-layered hollow cylinder by using the Green's function method', J. Appl. Math. & Comput. Mech. 12 (2013) 45–50.
[17] H. Qian, D. Zhou, W. Liu, W. Lu, H. Feng, Thermal stresses in layered thick cylindrical shells of infinite length, J. Therm. Stresses 40 (2017) 322–343.
[18] M.H. Kayhani, M. Norouzi, A. Amiri Delouei, A general analytical solution for heat conduction in cylindrical multilayer composite laminates, Int. J. Therm. Sci. 52 (2012) 73–82.
[19] F. Erchiqui, Z. Annasabi, 3D hybrid finite element enthalpy for anisotropic thermal conduction analysis, Int. J. Heat Mass Tran. 136 (2019) 1250–1264.
[20] Z. Annasabi, F. Erchiqui, 3D hybrid finite elements for anisotropic heat conduction in a multi-material with multiple orientations of the thermal conductivity tensors, Int. J. Heat Mass Tran. 158 (2020) 1–12, 119795.
[21] C.-C. Ma, S.-W. Chang, Analytical exact solutions of heat conduction problems for anisotropic multi-layered media, Int. J. Heat Mass Tran. 47 (2004) 1643–1655.
[22] A. Zukauskas, J. Ziugzda, Heat Transfer of a Cylinder in Crossflow, Hemisphere Publishing, New York, 1985.
[23] E. Schmidt, K. Wenner, 'Heat Transfer over the Circumference of a Heated Cylinder in Transverse Flow,' National Advisory Committee for Aeronautics (NACA) Technical Report NACA-TM-1050, 1943 last accessed 2020/05/15, https://ntrs.nasa.gov/search.jsp?R=20000043165.
[24] D. Sarkar, K. Shah, A. Haji-Sheikh, A. Jain, Analytical modeling of temperature distribution in an anisotropic cylinder with circumferentially-varying convective heat transfer, Int. J. Heat Mass Tran. 79 (2014) 1027–1033.
[25] D. Sarkar, K. Shah, A. Haji-Sheikh, A. Jain, Thermal conduction in an orthotropic sphere with circumferentially varying convection heat transfer, Int. J. Heat Mass Tran. 96 (2016) 406–412.
[26] S. Drake, M. Martin, D. Wetz, J. Ostanek, S. Miller, J. Heinzel, A. Jain, Heat generation rate measurement in a Li-ion cell at large C-rates through temperature and heat flux measurements, J. Power Sources 285 (2015) 266–273.
[27] S. Drake, M. Martin, D. Wetz, J. Ostanek, S. Miller, J. Heinzel, A. Jain, Measurement of anisotropic thermophysical properties of cylindrical Li-ion cells, J. Power Sources 252 (2014) 298–304.